Calibration of binding energy and clarification of interfacial band bending for Al_2O_3/diamond heterojunction

J. W. Liu,[1, a)] T. Teraji,[1] B. Da,[2] and Y. Koide[1]

[1]*Research Center for Electronic and Optical Materials, National Institute for Materials Science (NIMS), 1-1 Namiki, Tsukuba, Ibaraki 305-0044, Japan*

[2]*Research and Services Division of Materials Data and Integrated System, NIMS, 1-1 Namiki, Tsukuba, Ibaraki 305-0044, Japan*

[a)] Author to whom correspondence should be addressed; electronic mail: liu.jiangwei@nims.go.jp

Abstract

Due to the presence of an intrinsic C 1*s* peak in diamond, it is impossible to calibrate its binding energies using the adventitious C 1*s* peak (284.8 eV) during X-ray photoelectron spectroscopy measurement. The absence of accurate binding energy measurement makes it challenging to determine the interfacial band bending for the oxide/diamond heterojunction. To overcome this issue, a net-patterned gold (Au) mask is applied to the boron-doped diamond (B-diamond) to suppress the charge-up effect and calibrate the binding energy using the standard Au 4*f* peak (83.96 eV). The B-diamond epitaxial layer shows downward band bending towards the surface with valence band maximum of 0.85 eV. Upon the formation of Al_2O_3 using an ozone precursor through the atomic layer deposition technique, the B-diamond continues to exhibit downward band bending towards the Al_2O_3/B-diamond interface. However, the bending energy has reduced, potentially attributed to the modification of the oxygen vacancies on the B-diamond surface by the ozone precursor during the Al_2O_3 deposition.

1 Carbon-related material of diamond has unique properties such as wide bandgap
2 energy, high thermal conductivity, high breakdown voltage, good chemical stability, and
3 radiation hardness.[1-3] These properties make it suitable for applications in fields of high-
4 power, high-frequency, high-temperature, and harsh environments. Diamond-based
5 electronic devices, such as diamond metal-oxide-semiconductor (MOS) capacitors[4, 5] and
6 MOS field-effect transistors (MOSFETs),[6-8] have been developed and show promise in
7 high-power, high-frequency, and high-temperature applications.

8 For fabricating high-performance diamond-based MOS capacitors and MOSFETs,
9 understanding the band configuration at the oxide/diamond interface is crucial.[9] It can
10 help in optimizing the leakage current density and charge storage properties for the
11 diamond MOS capacitors. It can also help to understand the threshold voltage, charge
12 injection and extraction, and device stability for the diamond MOSFETs.[10] Thus,
13 clarification the band configuration for the insulator/diamond interface is important for
14 designing and fabricating more efficient and reliable diamond-based MOS electronics.

15 There are several techniques used to investigate the band configurations at the
16 oxide/semiconductor interface, such as X-ray photoelectron spectroscopy (XPS),[11, 12]
17 capacitance-voltage measurement,[13] current-voltage measurement,[14] and Kelvin probe
18 force microscopy.[15] Comparing other techniques, the XPS offers valuable advantages
19 such as providing chemical information, band bending analysis, non-destructive
20 measurements, and compatibility with different materials.

21 Band offsets for different oxide insulators on hydrogen-terminated diamond and
22 boron-doped diamond (B-diamond) have been demonstrated using the XPS technique.[16,
23 17] However, the presence of the intrinsic C 1*s* peak in diamond makes it impossible to
24 calibrate the binding energy using the adventitious C 1*s* peak (284.8 eV), which makes it

difficult to clarify the interfacial band bending for the oxide/diamond heterojunctions.

In this letter, a net-patterned gold (Au) mask is formed on the B-diamond to suppress the charge-up effect and allows for the calibration of the binding energies using the standard Au 4*f* peak (83.96 eV). The surface band bending for the B-diamond and interfacial band bending for the Al_2O_3/B-diamond heterojunction would be clarified.

Figure 1 illustrates the process of forming the net-patterned Au mask and the Al_2O_3 insulator on the B-diamond. The Ib-type (100) diamond substrate was immersed in a solution of H_2SO_4 + HNO_3 at 300 °C for 3 hours to clean the surface. The B-diamond epitaxial layer was then grown using microwave plasma-assisted chemical vapor deposition technique [Fig. 1(a)]. The microwave power, temperature, and chamber pressure were maintained at 1.4 kW, approximately 1000 °C, and 18.6 kPa, respectively.[18] The boron source used was the residual boron in the chamber from the previous B-diamond growth. The flow rates for the source gases of H_2 and CH_4 were set at 49 and 1 sccm, respectively. The thickness and boron atom concentration of the B-diamond epitaxial layer was measured by secondary ion mass spectroscopy and found to be 825 nm and 4×10^{15} cm^{-3}, respectively.

The B-diamond epitaxial layer was treated in an acid solution of H_2SO_4 + HNO_3 at 300 °C for 3 hours again, resulting in a transformation of its hydrogen-terminated surface to an oxygen-terminated surface. Following the treatment, the oxygen-terminated B-diamond epitaxial layer was cleaned sequentially with acetone, ethanol, and pure water. The first-time high-resolution XPS measurement (Instrument: PHI Quantera SXM, ULVAC-PHI) was conducted. Valence band and core level spectra were obtained for the B-diamond without the Au mask. The X-ray source employed was monochromate Al Kα (hv =1486.6 eV) with a take-off angle of 45°, a power output of 50 W, a measurement

1 area of 200 μm, a pass energy of 55 eV, and an energy step of 0.1 eV.

2 A laser lithography system and electron-gun evaporation equipment were utilized to
3 create the net-patterned Au mask on the B-diamond [Fig. 1(b)]. The B-diamond was
4 coated sequentially with a positive photoresist (LOR5A) and an image reversal
5 photoresist (AZ5214E) using a spin-coater. The spin speed and time for coating both
6 photoresists were set at 7000 rpm and 1 second, respectively. The LOR5A was baked at
7 180 °C for 5 minutes, while the AZ5214E was baked at 110 °C for 2 minutes.
8 Subsequently, it underwent exposure and development processes using a DL-1000
9 scanning maskless lithography system and a tetramethylammonium hydroxide (TMAH)
10 solution with a concentration of 2.38%. The developing time in the TMAH solution was
11 2.5 minutes. A 100 nm-thick Au mask and position correction cross patterns ("+") were
12 formed on the B-diamond. The evaporation chamber pressure was approximately 10^{-6} Pa
13 with an evaporation rate of 2 Å/s. The second time XPS measurement was conducted to
14 obtain core level spectra for the B-diamond with the Au mask.

15 A 3 nm-thick Al_2O_3 insulator was deposited on the entire surface of the B-diamond
16 with the Au mask using an atomic layer deposition system. The deposition involved the
17 use of $Al(CH_3)_3$ and ozone precursors at a temperature of 200 °C [Fig. 1(c)]. Subsequently,
18 a window was opened in the Al_2O_3 film to expose the Au mask by etching with the TMAH
19 solution at room temperature for 12 minutes [Fig. 1(d)]. The third time XPS measurement
20 was then performed to capture the core level spectra for the Al_2O_3 and B-diamond with
21 the Au mask. It should be noted that a 30 nm-thick Al_2O_3 film was deposited on a silicon
22 substrate to provide additional information on the valence band and core level spectra,
23 which can be calibrated with the adventitious C 1*s* peak (284.8 eV) and were crucial for
24 deducing the band offsets of the Al_2O_3/B-diamond heterojunction.

Figures 2(a) and 2(b) display the scanning electron microscopy image and scanning X-ray image, respectively, of the Al_2O_3 (3 nm)/B-diamond with the Au mask. The B-diamond exhibits a net-patterned Au mask with 10 position correction cross patterns ("+"). The side length of the square grid is 200 μm, and the center of the X-ray is positioned at the Al_2O_3/B-diamond. The spectra for Au, Al_2O_3, and B-diamond can be simultaneously obtained from this configuration.

Figure 3(a) presents the as-received C 1*s* spectra for the B-diamond without (black line) and with (red line) the Au mask. The corresponding binding energies are measured as 283.23 eV and 284.50 eV, respectively. The binding energy difference (ΔE) of 1.27 eV indicates the presence of a charge-up effect[19] on the B-diamond epitaxial layer with the low doping level. In Fig. 3(b), the as-received Au $4f_{7/2}$ spectra are shown for the B-diamond and the Al_2O_3/B-diamond samples with the Au mask. For the B-diamond with the Au mask, the binding energy of the as-received Au $4f_{7/2}$ spectrum is measured as 83.97 eV, which closely matches the ideal value of 83.96 eV. This suggests that there is almost no charge-up effect on the B-diamond with the Au mask during the XPS measurement. However, for the Al_2O_3/B-diamond with the Au mask, the binding energy shifts to a higher value of 84.15 eV. This shift arises from the accumulation of negative charges on the sample surface due to the charge-up effect. Despite the presence of the Au mask, the charge-up effect on the Al_2O_3/B-diamond cannot be eliminated.

Therefore, the presented results indicate the existence of a charge-up effect on the low doping level B-diamond epitaxial layer, as evidenced by the significant binding energy difference between the spectra without and with the Au mask. While the charge-up effect is minimal for the B-diamond sample with the Au mask, it remains pronounced for the Al_2O_3/B-diamond sample, necessitating the calibration of peak binding energies

1 for accurate analysis.

2 Figure 4(a) shows the calibrated C 1*s* spectra for B-diamond and Al_2O_3(3 nm)/B-
3 diamond with the Au mask. The main peak corresponding to carbon-carbon (C-C) bonds
4 in the C 1*s* spectrum of B-diamond is observed at a binding energy of 284.50 eV. Upon
5 depositing Al_2O_3 on B-diamond, the peak shifts to a lower binding energy of 284.15 eV,
6 resulting in a shift of $\Delta E = 0.35$ eV. Additionally, a peak at approximately 284.5 eV in the
7 Al_2O_3(3 nm)/B-diamond spectrum is attributed to carbon-boron (C-B) bonds.[20] In Fig.
8 4(b), the calibrated valence band spectra for B-diamond without an Au mask and Al_2O_3(30
9 nm)/Si are shown. Due to the potential impact of the Au mask on determining the valence
10 band maximum (VBM) of B-diamond, we opted to use B-diamond samples without an
11 Au mask for VBM determination. By extrapolating linear fittings for the leading edge to
12 the baseline, the valence band maximum (VBM) values are determined to be 0.85 eV for
13 B-diamond and 3.38 eV for Al_2O_3 (30 nm). Fig. 4(c) displays the calibrated Al 2*p* spectra
14 for the Al_2O_3(3 nm)/B-diamond and Al_2O_3(30 nm)/Si samples. The main peaks
15 corresponding to aluminum-oxygen (Al-O) bonds are observed at binding energies of
16 72.99 eV and 74.57 eV, respectively. In the Al_2O_3(30 nm)/Si spectrum, a peak at
17 approximately 77.0 eV is attributed to surface aluminum-oxygen-hydroxide (Al-O-OH)
18 bonds.[21]

19 The valence band offset (VBO) of the Al_2O_3/B-diamond heterojunction can be
20 calculated using equation (1) below:

21 $$VBO = (E_{C\,1s} - E_{VBM})_{B-diamond} - (E_{Al\,2p} - E_{VBM})_{Al_2O_3\,(30\,nm)}$$

22 $$- (E_{C\,1s} - E_{Al\,2p})_{Al_2O_3\,(3\,nm)}$$

23 The term $(E_{C\,1s} - E_{VBM})_{B-diamond}$ represents the difference in binding energy between
24 the C 1*s* level and the VBM for the B-diamond, which has a value of 283.65 eV. The term

1 $(E_{Al\ 2p} - E_{VBM})_{Al_2O_3\ (30\ nm)}$ represents the difference in binding energy between the Al 2 $2p$ level and the VBM for a 30 nm thick Al_2O_3 layer, which is 71.19 eV. Finally, the term 3 $(E_{C\ 1s} - E_{Al\ 2p})_{Al_2O_3\ (3\ nm)}$ represents the difference in binding energy between the C $1s$ 4 level and the Al $2p$ level for a 3 nm thick Al_2O_3 layer, which amounts to 211.16 eV. By 5 substituting the given values into equation (1), the VBO for the Al_2O_3/B-diamond 6 heterojunction can be calculated as 1.30 eV, which is in good agreement with the previous 7 report.[16] Additionally, based on the provided bandgap energies of diamond (5.47 eV) and 8 Al_2O_3 (7.2 eV),[11] the conduction band offset (CBO) for the Al_2O_3/B-diamond 9 heterojunction can be inferred to be 0.43 eV.

10 Figure 4(d) illustrates schematic band diagram for the Al_2O_3/B-diamond 11 heterojunction, exhibiting a type I straddling band configuration. Based on a doping 12 concentration of 4×10^{15} cm^{-3}, the Fermi level potential in the bulk B-diamond is 13 estimated to be approximately 0.37 eV.[22] In the case of B-diamond, the presence of 14 oxygen vacancies or native defects results in positive charges on the surface, causing a 15 downward band bending towards the surface with the VBM of 0.85 eV. Upon the 16 formation of Al_2O_3 using an ozone precursor through the ALD technique, the B-diamond 17 continues to exhibit downward band bending towards the Al_2O_3/B-diamond interface. 18 However, the bending energy has reduced, potentially attributed to the modification of 19 the ozone precursor with regards to the oxygen vacancies.

20 In conclusion, a new technique was developed to obtain precise binding energies for 21 B-diamond and Al_2O_3/B-diamond. The band bending and band configuration for the 22 Al_2O_3/B-diamond were clarified. An Au mask was applied to the B-diamond to suppress 23 the charge-up effect and calibrate the binding energy using the standard Au $4f$ peak. The 24 B-diamond shows downward band bending towards the surface with the VBM of 0.85 eV.

Upon the formation of Al_2O_3 using an ozone precursor through the ALD technique, the B-diamond continues to exhibit downward band bending towards the Al_2O_3/B-diamond interface. However, the extent of bending has reduced. This technique is also applicable for obtaining precise binding energies for other carbon-related materials.

This work is supported by the JSPS KAKENHI Projects (JP23K03966, 20H05661, and JP20H00313), MEXT Q-LEAP (JPMXS0118068379), JST CREST (JPMJCR1773), JST Moonshot R&D (JPMJMS2062), MIC R&D for construction of a global quantum cryptography network (JPMI00316), and ARIM (JPMXP1223NM5006) of the Ministry of Education, Culture, Sports, Science and Technology, Japan.

Data Availability Statements

The data that support the findings of this study are available from the corresponding author upon reasonable request.

1 **References**

2 1. M. Geis, Mat. Res. Soc. Symp. Proc. **162**, 15 (1990).
3 2. C. J. H. Wort and R. S. Balmer, Mater. Today **11**, 22 (2008).
4 3. H. Umezawa, Mater. Sci. Semi. Proc. **78**, 147 (2018).
5 4. J. Liu, M. Liao, M. Imura, H. Oosato, E. Watanabe, and Y. Koide, Appl. Phys. Lett.
6 **102**, 112910 (2013).
7 5. J. Liu, H. Oosato, B. Da, and Y. Koide, Appl. Phys. Lett. **117**, 163502 (2020).
8 6. K. Hirama, H. Sato, Y. Harada, H. Yamamoto, and M. Kasu, Jpn. J. Appl. Phys. **51**,
9 090112 (2012).
10 7. W. Wang, Y. Wang, M. Zhang, R. Wang, G. Chen, X. Chang, F. Lin, F. Wen, K. Jia,
11 and H. X. Wang, IEEE Electron Dev. Lett. **41**, 585 (2020).
12 8. W. Fei, T. Bi, M. Iwataki, S. Imanishi, and H. Kawarada, Appl. Phys. Lett. **116**,
13 212103 (2020).
14 9. J. Robertson, J. Vac. Sci. Technol. B **18**, 1785 (2000).
15 10. J. Goo, Q. Xiang, Y. Takamura, F. Arasnia, E. N. Paton, P. Besser, J. Pan, and M.
16 Lin, IEEE Electron Dev. Lett. **24**, 568 (2003).
17 11. J. W. Liu, M. Y. Liao, M. Imura, and Y. Koide, Appl. Phys. Lett. **101**, 252108 (2012).
18 12. J. Cañas, G. Alba, D. Leinen, F. Lloret, M. Gutierrez, D. Eon, J. Pernot, E. Gheerae
19 rt, and D. Araujo, Appl. Surf. Sci. **535,** 146301 (2021).
20 13. Y. Nemirovsky, G. Gordon, and D. Goren, J. Appl. Phys. **84**, 1113 (1998).
21 14. Z. Xu, M. Houssa, S. D. Gendt, and M. Heyns, Appl. Phys. Lett. **80**, 1975 (2002).
22 15. W. Melitz, J, Shen, A. C. Kummel, and S. Lee, Surf. Sci. Reports **66**, 1 (2011).
23 16. A. Marechal, M. Aoukar, C. Vallee, C. Riviere, D. Eon, J. Pernot, and E. Gheeraert,
24 Appl. Phys. Lett. **107**, 141601 (2015)
25 17. J. Liu, and Y. Koide, Sensors **18**, 1813 (2018).
26 18. T. Teraji, T. Yamamoto, K. Watanabe, Y. Koide, J. Isoya, S. Onoda, T. Ohshima, L.
27 J. Rogers, F. Jelezko, P. Neumann, J. Wrachtrup, and S. Koizumi, Physica Status
28 Solidi A **212**, 2365 (2015).
29 19. J. A. C. Santana, Quantitative Core Level Photoelectron Spectroscopy, Online
30 ISBN: 978-1-6270-5306-8, Morgan & Claypool Publishers (2015)

20. T. Yokoya, E. Ikenaga, M. Kobata, H. Okazaki, K. Kobayashi, A. Takeuchi, A. Awaji, Y. Takano, M. Nagao, I. Sakaguchi, T. Takenouchi, K. Kobayashi, H. Kawarada, and T. Oguchi, Phys. Rev. B **75**, 205117 (2007).
21. W. Liang, K. J. Weber, D. Suh, J. Yu, and J. Bullock, 2013 IEEE 39th Photovoltaic Specialists Conference, Tampa, FL, USA,16-21 June 2013.
22. A. T Collins, J. Phys.: Condens. Matter **14**, 3743 (2002).

Figure captions

FIG. 1. Process of forming the Au mask and the Al_2O_3 insulator on the B-diamond: (a) Diamond cleaning and B-diamond growth, (b) net-patterned Au mask, (c) Al_2O_3 deposition, and (d) opening windows for the Au mask.

FIG. 2. (a) Scanning electron microscopy image and (b) scanning X-ray image for Al_2O_3/B-diamond with the Au mask.

FIG. 3. (a) As-received C 1*s* spectra for the B-diamond without (black line) and with (red line) the Au mask, and (b) as-received Au $4f_{7/2}$ spectra for the B-diamond and the Al_2O_3/B-diamond samples with the Au mask.

FIG. 4. (a) Calibrated C 1*s* spectra for B-diamond and Al_2O_3(3 nm)/B-diamond with the Au mask, (b) calibrated valence band spectra for B-diamond without an Au mask and Al_2O_3(30 nm)/Si sample, (c) calibrated Al 2*p* spectra for the Al_2O_3(3 nm)/B-diamond and Al_2O_3(30 nm)/Si samples, and (d) schematic band diagram for the Al_2O_3/B-diamond heterojunction.

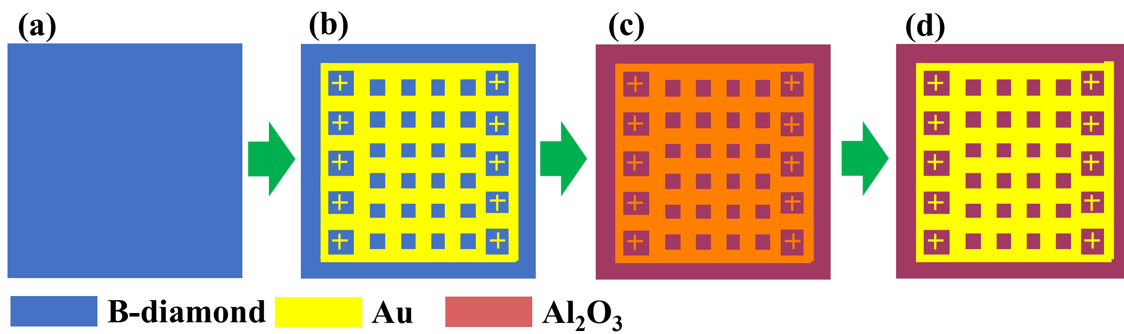

1

2

3

4 Liu *et al.*, Figure 1

5

6

7

8

9

10

11

12

13

14

15

16

17

18

19

1

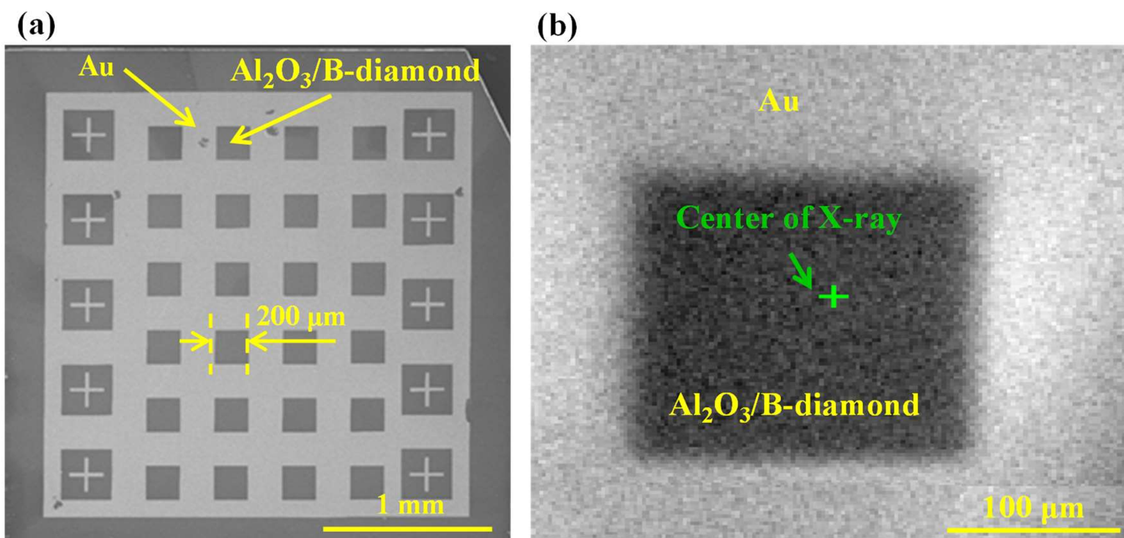

2

3

4 Liu *et al.*, Figure 2

5

6

7

8

9

10

11

12

13

14

15

16

17

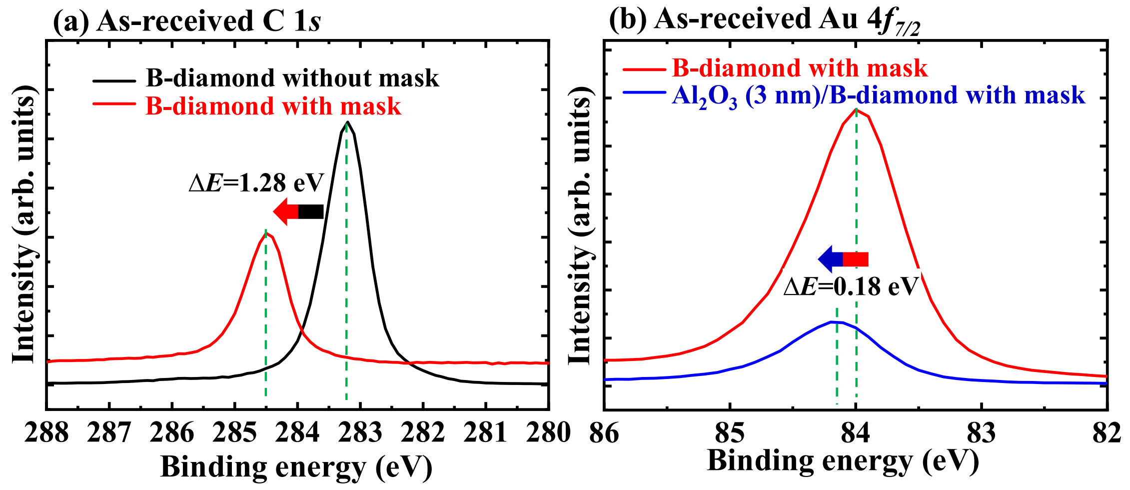

1

2

3

4 Liu *et al.*, Figure 3

5

6

7

8

9

10

11

12

13

14

15

16

17

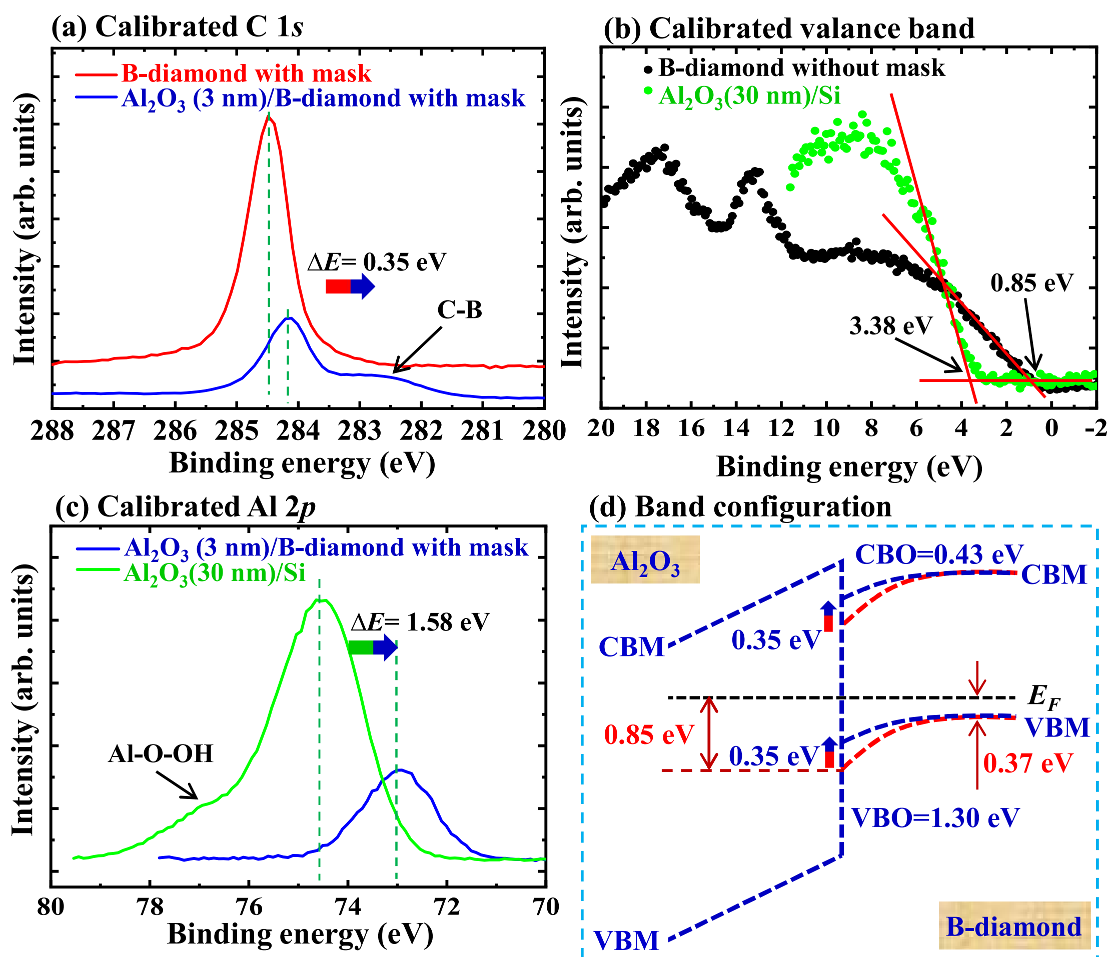

1

2

3

4

5 Liu *et al.*, Figure 4

6

7